Earth and Planetary Science Letters 349-350 (2012) 67–74

Contents lists available at SciVerse ScienceDirect

Earth and Planetary Science Letters

journal homepage: www.elsevier.com/locate/epsl

Letters

Flattening the Bhutan Himalaya

Stacey L. Corrie [a,*], Matthew J. Kohn [a], Nadine McQuarrie [b], Sean P. Long [c]

[a] Department of Geosciences, Boise State University, Boise, ID 83725, USA
[b] Department of Geology and Planetary Science, University of Pittsburgh, Pittsburgh, PA 15260, USA
[c] Nevada Bureau of Mines and Geology, University of Nevada, Reno, NV 89557, USA

ARTICLE INFO

Article history:
Received 27 April 2012
Received in revised form
29 June 2012
Accepted 2 July 2012
Editor: T.M. Harrison
Available online 27 July 2012

Keywords:
Bhutan
flattening
Himalaya
strain
thermobarometry

ABSTRACT

A detailed thermobarometric transect of 35 samples across the Greater and Tethyan Himalayan sequences in central Bhutan demonstrates a tectonostratigraphically-intact section with uniform apparent thermal and baric field gradients of 20 ± 2 °C/km and 0.57 ± 0.08 kbar/km. Pressure–temperature paths determined from chemically-zoned garnets in 6 samples demonstrate that these *P–T* conditions correspond with maximum pressures. The super-lithostatic baric gradient cannot be explained by pre- to syn-metamorphic tectonic processes, or by extension within an inclined slab. Instead the data imply 50% post-peak-metamorphic flattening of the Himalayan metamorphic core, accommodated by distributed, top-to-the-north shear, consistent with microstructural analysis. Orogenic flattening best explains the development of the South Tibetan Detachment System as a strain incompatibility feature rather than a structure bounding the top of a tectonically-inserted wedge, and helps reconcile debate attributing first-order Himalayan structural features to either wedge failure ("critical taper") or pipe-flow ("channel flow").

1. Introduction

The Himalayan mountain belt, which has been forming in response to the Indo-Asia collision since ~55 Ma (Rowley, 1996), is regarded as a classic continent–continent collisional orogen. Orogen-scale flattening has been proposed as an important mechanical process in the Himalaya (e.g., Burchfiel and Royden, 1985; Law et al., 2004; Long et al., 2011a), but structural measurements alone do not quantitatively constrain its magnitude. To further our knowledge of the degree of orogenic flattening in the Himalaya, we present the first detailed thermobarometric transect across the Greater and Tethyan Himalayan sequences in Bhutan (Figs. 1 and 2) to assess current models of development of the South Tibetan Detachment System (STDS). These models depend upon our understanding of the tectonic and metamorphic evolution of the Himalaya, which has implications for the evolution of orogens in general. Our transects cross the axis of a broad, approximately east–west trending syncline (Fig. 2), and sample structural distances of nearly 10 km both to the north and south of the fold axis. The regional geology of this area is discussed extensively elsewhere (Long and McQuarrie, 2010; Long et al., 2011a,c).

Flattening, a form of coaxial shear with two comparable elongation directions and one shortening direction, is commonly inferred from shapes of deformed sedimentary clasts, preferred crystal axis orientations, or boudinaged horizons. Extrapolating thin-section, hand-sample or outcrop-scale features to an entire orogen, however, remains problematic for two reasons related to the scale of observation. First, material that has been displaced adjacent to a flattened feature may be unrecognizably redistributed within the same rock, so the flattening recorded by one physical component may not be representative of the bulk strain that the entire rock experienced. Second, even if a specific rock has undergone flattening, we cannot know whether that rock is representative of an entire section: continuous quantitative strain measurements through km or tens of km of section are not currently possible. For example, recent detailed micro- and macro-structural studies of strain in the Himalaya examined on average 3–5 samples per km structural thickness (Law et al., 2004; Long et al., 2011a). Assuming that each sample spanned a 20 cm interval, ca. 99.9% of each section remains structurally unquantified, implying ~1000:1 extrapolations.

In contrast to strain, which is an extensive property of rocks, pressure and temperature are continuous, intensive properties that can be interpolated between samples more confidently. Thus *P–T* distributions and *P–T* path evolution allow us to infer broad-scale tectonic processes more confidently from a necessarily limited number of observations. In this study, we used conventional thermobarometry and differential thermodynamics to determine the distribution of pressures and temperatures through a thick section of exposed crust as well as pressure–temperature trajectories in rock amenable to such calculations. As we develop in later sections, we interpret our data as indicating that the 9.3 km thick section we studied in Bhutan was originally $\sim 19 \pm 2$ km thick, and that approximately 50% flattening occurred. We then evaluate whether our data

* Corresponding author. Tel.: +1 208 426 2523; fax: +1 208 426 4061.
E-mail addresses: staceycorrie@boisestate.edu (S.L. Corrie), mattkohn@boisestate.edu (M.J. Kohn), nmcq@pitt.edu (N. McQuarrie), splong@unr.edu (S.P. Long).

0012-821X/$ - see front matter © 2012 Elsevier B.V. All rights reserved.
http://dx.doi.org/10.1016/j.epsl.2012.07.001

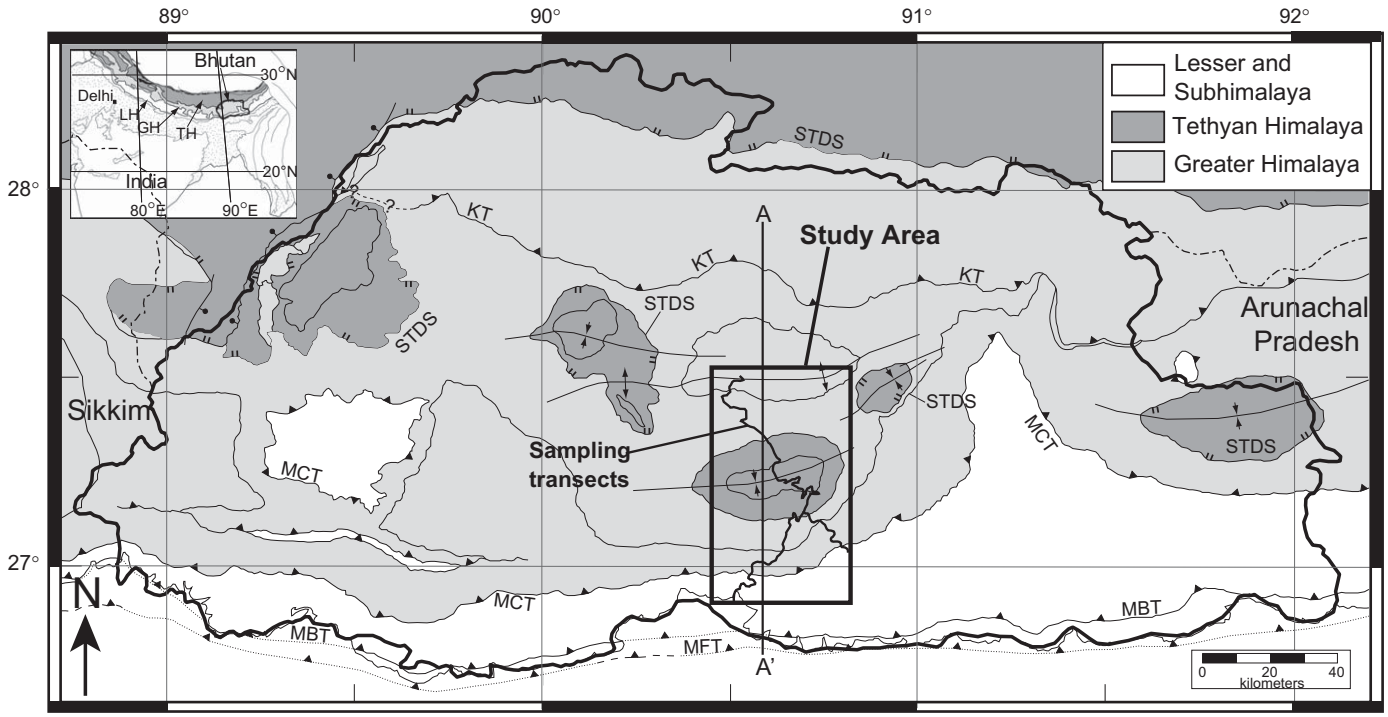

Fig. 1. Simplified geologic map of Bhutan (Long et al., 2011b), showing main lithotectonic units and structures. Structures with triangular teeth on hanging wall are thrusts (KT=Kakhtang thrust, MBT=Main Boundary Thrust, MCT=Main Central Thrust, MFT=Main Frontal Thrust); structures with either balls or double tic-marks are normal faults or shear zones (STDS=South Tibetan Detachment System).

and their implications for post-peak-metamorphic changes to crustal thickness are consistent with previously proposed models for the evolution of the Himalayan tectonic wedge, particularly with respect to flattening and strain distributions.

In the Himalaya, three endmember models of crustal deformation have emerged. In channel flow (Grujic et al., 1996; Beaumont et al., 2001; Jamieson et al., 2004), a central channel exhibiting pipe-flow occurs, with normal- and thrust-sense shear zones along its upper and lower bounds (Fig. 3A). The thickness of the normal-sense shear zone may vary depending on the degree of coupling (rheological contrast) with the extruding channel although extensive coupling minimizes extrusion magnitudes (Beaumont et al., 2004). In critical taper (Fig. 3B; Davis et al., 1983; Dahlen, 1990; Robinson et al., 2006; Kohn, 2008), the orogenic wedge is everywhere critically failing. Changes to internal strength (e.g., from metamorphic reactions) or boundary conditions may cause the wedge to thicken or extend, and in principle both compressional and extensional features may develop simultaneously, either as discrete structures or distributed within the wedge. Although flattening and extensional shear are commonly attributed to channel flow (e.g., Jamieson et al., 2004; Law et al., 2004), critical taper also permits such features. A third model, tectonic wedging (Webb et al., 2007; Fig. 3C), has similar shear sense kinematics as channel flow, but the bounding shear zones merge updip, and flattening is not specifically predicted.

2. Materials and methods

2.1. Electron probe microanalysis

Elemental compositions for all minerals of thermobarometric interest and X-ray maps of garnet and surrounding matrix were collected using the Cameca SX-100 electron microprobe housed in the Department of Earth and Environmental Sciences at the Rensselaer Polytechnic Institute, Troy, New York, and the JEOL JXA 8200 at the Lawrence Livermore National Laboratory. Natural and synthetic silicates and oxides were used for calibrations, and quantitative measurements were made using an accelerating voltage of 15 kV and a current of 20 nA (major silicates) or 100 nA (rutile). Beam sizes were 10 μm for plagioclase and micas, 2 μm for rutile, and minimum for garnet. Peak count times were 10 s (Na, Ca, Fe, Mn, Si, Al), 20 s (Mg, Ti, K), and 45 s (Zr in rutile; one sample only). X-ray maps for Fe, Mg, Mn, Ca, and Al in garnet were collected with an accelerating voltage of 15 kV, current of 200 nA, pixel time of 30 ms, minimum beam size, and step size of 2–6 μm/pixel.

Mineral compositions reflective of peak metamorphic conditions were selected using standard petrologic criteria (Kohn and Spear, 2000; Kohn et al., 1992, 1993; Spear et al., 1990a; Spear, 1991, 1995). These methods account for possible retrograde garnet dissolution and Fe–Mg exchange with other matrix minerals. The garnet–biotite thermometer of Ferry and Spear (1978) with the Berman (1990) garnet solution model was used for most samples except K11B019 and BU08-87, in which the garnet–hornblende thermometer (Graham and Powell, 1984) and the Zr-in-rutile thermometer (Watson et al., 2006; Tomkins et al., 2007) were used, respectively. Depending on the mineral assemblage of the sample, pressures were calculated using the garnet–plagioclase–aluminosilicate–quartz barometer (Koziol and Newton, 1988) with the Berman (1990) garnet solution model, the garnet–plagioclase–muscovite–biotite barometer (Hoisch, 1990), or the garnet–plagioclase–hornblende–quartz barometer (Kohn and Spear, 1990). *P–T* conditions and mineral compositions are reported in Tables S1–S5.

2.2. P–T path calculations

P–T paths were calculated using differential thermodynamics (the Gibbs method; Spear, 1995). We restricted consideration to relatively low-grade rocks containing the assemblage garnet+biotite+muscovite+plagioclase+quartz ± chlorite in the system $MnO–Na_2O–CaO–K_2O–FeO–MgO–Al_2O_3–SiO_2–H_2O$. Assuming pure

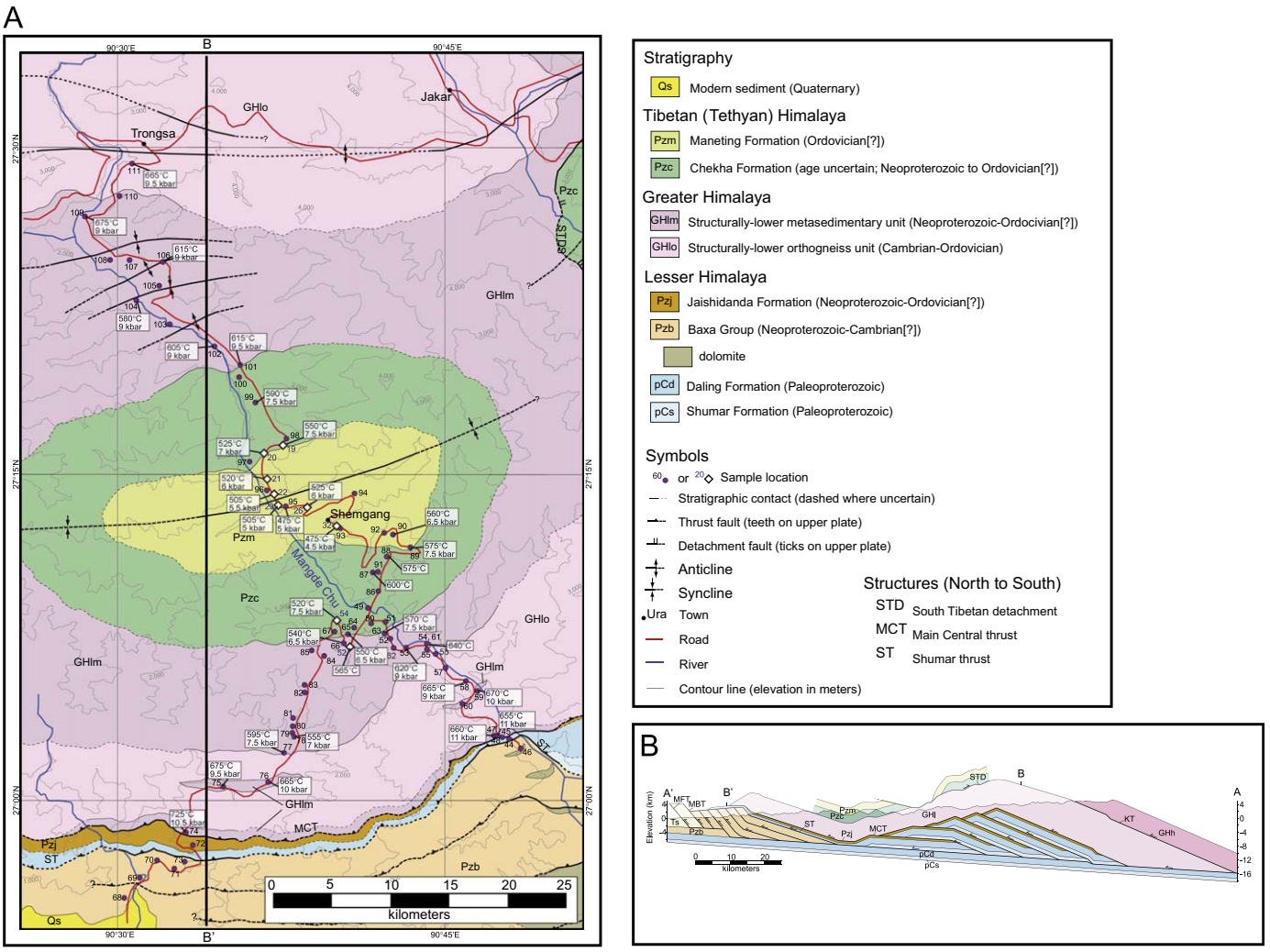

Fig. 2. (A) Geologic map of the Shemgang area, Bhutan (from Long et al., 2011c), where detailed *P–T* calculations were determined. Dots and diamonds show sample locations with BU08- and K11B-prefixes, respectively. (B) Cross-section through line B-B′ (modified from Long et al., 2011a). Note that structurally-lower Greater Himalayan section is simplified to GHl.

H_2O and chlorite during garnet growth, this assemblage has a thermodynamic variance of 4. Two rocks do not contain prograde chlorite, so we assumed chlorite compositions based on typical Fe–Mg–Mn partitioning observed between biotite and chlorite (Table S5). We examined only low-grade rocks to minimize bias due to diffusional exchange in higher grade rocks (Florence and Spear, 1991) and to ensure insofar as possible that garnet grew in chlorite-bearing assemblages. All garnets exhibit decreases in Mn and Fe/(Fe+Mg) from core to rim, and increases in Fe and Mg, and many rocks contain chlorite with equilibrium Fe/Mg/Mn relative to garnet and biotite, consistent with these considerations (Spear et al., 1990a).

Changes to *P* and *T* were determined based on observed garnet growth zoning and matrix plagioclase zoning (Table S5). In all cases, plagioclase shows an increase in X_{An} from the rim towards the core, although plagioclase in several rocks has lower X_{An} cores. Because growth of garnet is expected to preferentially consume the anorthite component of plagioclase (Spear et al., 1990a), we correlate only the outer region of plagioclase that exhibits the systematic decrease in X_{An} towards rims with garnet growth (Florence et al., 1993; Kohn et al., 1992; Spear et al., 1990b). The core region and step to higher X_{An} in some matrix plagioclase grains probably reflects growth in a different assemblage, e.g., carbonate- or epidote-bearing. Carbonate and epidote inclusions in garnet are common in carbonate- and epidote-stable assemblages, but no such inclusions were observed in any garnets in our study. Thus we assume these other calcic phases had broken down prior to garnet growth. Computationally, we used Gibbs OSX (downloaded from 〈http://ees2.geo.rpi.edu/MetaPetaRen/Software/Software.html〉) and the Gibbs tutorial thermodynamic database with ideal solutions, Fe–Mg–Mn mixing in biotite and chlorite, and Fe–Mg–Al mixing in muscovite. Use of different thermodynamic datasets and more complicated mixing models suggest minimal changes to calculated ΔP and ΔT (a few degrees and a few hundred bars). Because we have no direct way to correlate changes of plagioclase and garnet composition, we show 2-point paths for most rocks; the consistency of garnet zoning, however, suggests that pressures could not have been higher for lower grade rocks (K11B-32, BU08-95, K11B-21 and K11B-54). In the case of sample BU08-63, we explored the possibility that the zoning reflected a decrease in pressure with increasing temperature. Including mass balance constraints (reducing the variance to 2) suggests late-stage garnet growth might have occurred during isobaric heating, similar to the path inferred for sample BU08-89; we show the results of splitting the garnet into two compositional segments: core-mid and mid-rim. Regardless of specifics, the maximum pressure attained by both BU08-63 and -89 was not likely more than a few hundred bars higher than the rim pressure.

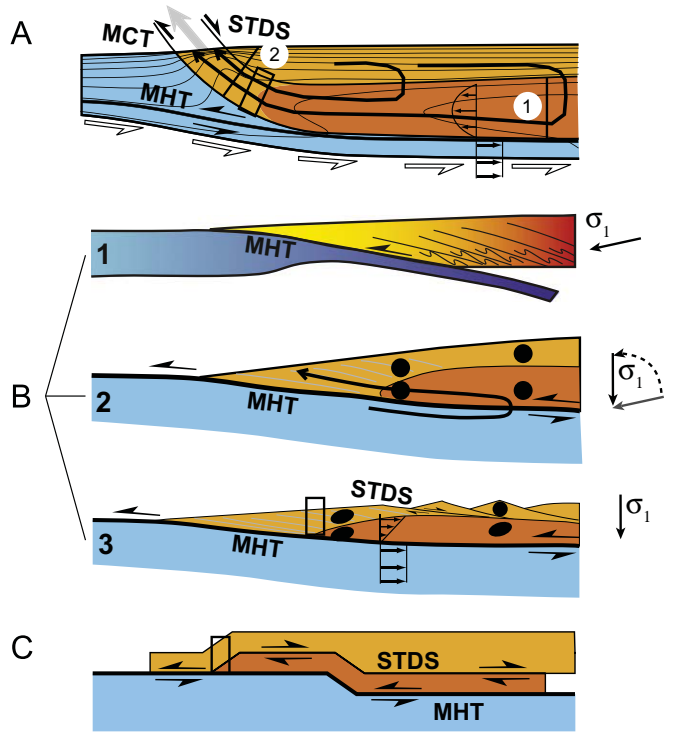

Fig. 3. Three main models of Himalayan structure and origins of STDS (adapted from Northrup, 1996; Jamieson et al., 2004; Godin et al., 2006; Webb et al., 2007). MHT=Main Himalayan Thrust, or basal shear zone; black symbols represent strain ellipses; arrows show direction of flow; boxes show corresponding region of study. (A) Channel flow model; channel (darker region) experiences pipe-flow and is bounded above by STDS. Flattening occurs as rocks move through channel (location 1 to 2). (B) Critical taper model; STDS forms during secular response to wedge weakening. (B1) Initially strong wedge with $\sigma 1$ (principal stress direction) subhorizontal. (B2) Wedge weakens as partial melting reactions are crossed or partial melts are underplated (darker region), causing rotation of $\sigma 1$ to subvertical as weakened rocks lose shear strength. (B3) Flattening; STDS forms in regions of heterogeneous flattening towards the hinterland, whereas homogeneous flattening occurs towards foreland. (C) Tectonic wedging model showing insertion of high-grade rocks (darker region).

2.3. Thermobarometric trends

Thermobarometric trends were determined simply by regressing P or T vs. structural distance. Possible discontinuities across lithologies were evaluated with piecewise regressions for the Maneting Formation (MF), Chekha Formation (CF), and Greater Himalayan sequence (GHS) (Fig. 2).

3. Results

Samples were collected in 2008 (Long and McQuarrie, 2010; samples with prefix BU08) and in 2011 (samples with prefix K11B) along traverses that span the entire GHS and the exposed thickness of the Tethyan sequence (CF and MF) (Fig. 2). Formation boundaries are based on marked changes in lithology, especially the dominance of thick-bedded, clean (mica-poor) quartzite in the CF. The CF and MF have classically been interpreted as Tethyan Himalayan lithologies (Gansser, 1983; Bhargava, 1995; Grujic et al., 2002). The base of the GHS is a thrust contact with Lesser Himalayan rocks – the Main Central thrust – that initiated at c. 20 Ma in western Bhutan (Tobgay et al., 2012). The upper contact between the GHS and CF has been interpreted either as a normal-sense shear zone (the South Tibetan Detachment System; STDS; Grujic et al., 2002) or a stratigraphically-continuous section through the CF and MF (Long and McQuarrie, 2010). The lower 2–3 km of the GHS exhibits top-to-the-south sense of shear, whereas the overlying c. 10 km of GHS, CF and MF show overprinting, post-peak-metamorphic, top-to-the-north sense of shear (Long and McQuarrie, 2010). Deformation temperature range estimates, primarily from quartz recrystallization microstructure (Long et al., 2011a), range from c. 700 °C at the base of the section, c. 600 °C at the last occurrence of leuocosome (which we infer to represent former partial melt resulting from muscovite dehydration-melting; see Davidson et al., 1997; Daniel et al., 2003), 450–500 °C for the upper GHS and CF, and 400–450 °C for the MF.

Peak metamorphic pressure and temperature decrease structurally upward, from c. 700 °C, 10–11 kbar at the base of the GHS to 475–500 °C, 5–6 kbar at the top of the MF (Fig. 4; Table S1). Leucosome observed in one of the structurally-lowest samples (BU08-74) is consistent with minimum temperatures of 700 °C for muscovite dehydration-melting (Spear et al., 1999). Scatter in P–T conditions reflects a combination of thermobarometric errors beyond compositional variation, and superposition of different transects with somewhat different P–T distributions. Most P–T paths show garnet growth with increasing P and T, whereas others show late-stage, nearly isobaric heating (Fig. 4C); thus, the thermobarometric results reflect the maximum P and T reached by each rock. The distributions of P and T show no obvious discontinuities. Predicted P–T differences across formation boundaries using piecewise regressions are 0.3 kbar and 5 °C at the CF–MF contact, and 0.1 kbar and 25 °C at the CF–GHS contact, versus regression uncertainties >0.5 kbar and >50 °C. However, consistent apparent T and P gradients of 20 ± 2 °C/km and 0.57 ± 0.08 kbar/km throughout the full section explain the data. Possibly a lithostatic P gradient occurs in the CF, although P and T slopes are not statistically different from the MF and GHS at 95% confidence.

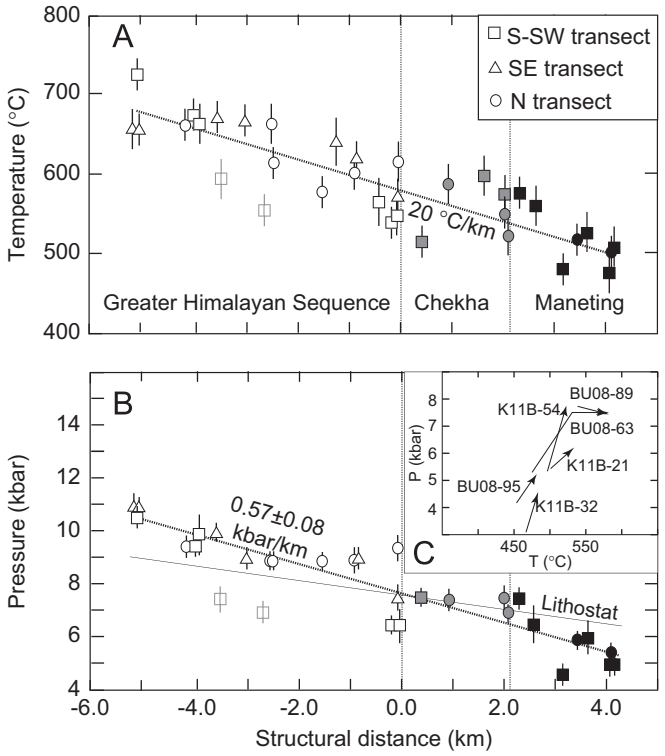

Fig. 4. (A) Temperature and (B) pressure vs. structural distance, showing uniform gradients throughout, and super-lithostatic baric gradient (0.57 ± 0.08 vs. 0.27 kbar/km). Vertical lines on symbols reflect thermobarometric range resulting from compositional variation. Two grayed outliers were omitted because of likely post-peak metamorphic re-equilibration. (C) Inset shows P–T paths determined from chemically zoned garnet crystals.

The overall apparent P gradient is two times steeper than lithostatic (c. 0.27 kbar/km, assuming an average upper crustal density of 2.8 g/cm^3). More specifically, an apparent pressure difference through the current 9.3 km thick section of 5.3 ± 0.6 kbar (2 s.e.) corresponds to a thickness of 19.2 ± 2.0 km. If this pressure gradient represents an original crustal thickness, then the section thickness has been homogeneously reduced after peak metamorphism by about 50% (range 46–56%). Distributing our peak temperature data over this 19.2 km thickness would further imply a low original thermal gradient of 9–10 °C/km. Note that low thermal gradients are intrinsic to eroding orogenic wedges (Royden, 1993), and have been predicted in the mid-crust by many Himalayan thermal-mechanical models (e.g., Beaumont et al., 2001, 2004; Henry et al., 1997; Herman et al., 2010; Royden, 1993). Post-metamorphic flattening is also consistent with quartz recrystallization temperatures < 500 °C for the upper GHS, CF, and MF (Long and McQuarrie, 2010; Long et al., 2011a), which are below peak thermobarometric estimates for nearly all rocks. The association of quartz recrystallization microstructures with top-to-the-north shear sense indicators suggests that any post-metamorphic flattening occurred simultaneously with north-directed shear.

4. Discussion

4.1. Is the GHS–THS contact the STDS?

The continuity of P–T conditions, P–T gradients, and P–T path shape across lithologic boundaries implies that lithologic contacts are essentially intact (Long and McQuarrie, 2010). Thus, neither the GHS–CF nor CF–MF contacts represents a shear zone over which structural displacement is recognized by a marked change in P or T conditions, e.g. the STDS (contra Grujic et al., 2002). Neither is there a change in P and T conditions within the GHS at the structural level where the change from top-to-the-south to top-to-the-north sense of shear is observed. This conclusion fundamentally changes interpretations of Himalayan geology, which have long assumed that the STDS underlies the Tethyan exposures and connects with exposures of the STDS farther north. As discussed elsewhere (Long and McQuarrie, 2010), either the STDS ramps to higher structural levels, is dissipated as distributed shear, or both. Any of these possibilities limit extensional shear to a few tens of km (Long and McQuarrie, 2010).

Other outlying exposures of THS above GHS (“klippen”) occur in Bhutan to the north and east of our study area. Some of these have ductile extensional shear structures localized at the THS–GHS boundary, and logically have been interpreted as ductile expressions of the STDS (Grujic et al., 2002; Kellett et al., 2010; Kellett and Grujic, 2012). The quantitative tectonic significance of these structures awaits more detailed petrologic and thermobarometric analysis.

In contrast to our data that show consistently low apparent thermal gradients (20 °C/km currently, 10 °C/km inferred for the restored state), high apparent thermal gradients up to several hundred °C/km characterize GHS–THS contacts elsewhere in Nepal and Bhutan (Cottle et al., 2011; Kellett and Grujic, 2012). These apparent gradients are interpreted to reflect thinning along the STDS and contrast markedly with our results.

4.2. Thermobarometric identification of post-peak-metamorphic flattening

Thermal models of collisional orogenesis and P–T path evolution in the context of Himalayan data (Fig. 5) ultimately recommend only one interpretation of the distribution of P–T conditions across the GHS and THS—that the section has been homogeneously flattened. Models of overthrusting (Fig. 5A and B) show that pressure gradients are expected to be lithostatic, sub-lithostatic, or even inverse, not super-lithostatic as observed. In classic overthrusting models (England and Thompson, 1984; Fig. 5A), deep-seated rocks experience more erosional exhumation before attaining peak P–T conditions, so their pressures record sub-lithostatic conditions relative to higher-level rocks. In continuous overthrusting models (Fig. 5B), typical of the Himalaya, a lithostatic pressure gradient is preserved in areas with constant wedge thickness, (rocks 1 and 2), and a sub-lithostatic or inverse pressure gradient in areas where the wedge thins (rocks 2 and 3). Such distributions are characteristic of thermobarometric transects in Nepal (Kohn, 2008; Corrie and Kohn, 2011). Both types of models imply younger metamorphic ages structurally downward, which is generally consistent with geochronologic results in Nepal (Kohn et al., 2004; Kohn, 2008; Corrie and Kohn, 2011). In contrast, chronologic data from Bhutan imply broadly coeval metamorphism through the GHS and THS (Daniel et al., 2003; Chambers et al., 2011; Kellett et al., 2010; Tobgay et al., 2012).

The only thrusting scenario that could produce a super-lithostatic pressure gradient would require that higher level rocks record an early low pressure and were later loaded along with deeper seated rocks, but somehow did not record the resulting pressure increase anywhere within the section. Petrological models (Spear et al., 1990a) demonstrate that, for the assemblages observed in our rocks, any increase in pressure would drive further garnet growth in Tethyan rocks and establish a lithostatic pressure gradient through the section. Thus we conclude that such a later pressure increase cannot have occurred during prograde metamorphism, and that thrusting is not responsible for the observed pressure distribution.

Effectively, thermobarometry shows that THS P's are much lower than anticipated from GHS P's and current structural thicknesses. Conventionally, the juxtaposition of low-P on high-P rocks would be interpreted in terms of extensional shear or thinning across an intervening structure. What distinguishes rocks in central Bhutan, however, is that the low-P on high-P juxtaposition does not occur across a discrete boundary, but is instead distributed through the section. This observation implies that thinning of this section also occurred homogeneously. This thinning could have occurred either as simple shear along inclined planes, possibly with some component of layer-normal pure shear (Fig. 5C), or as layer-normal pure shear within a horizontal crustal section, possibly with some component of simple shear (Fig. 5D). Channel flow predicts the simple shear-dominated scenario, in which an inclined basal thrust is coupled with extensional shear at higher structural levels. This model fails in the Himalaya for two reasons. First, geologic maps and accompanying cross-sections repeatedly demonstrate that the basal thrust emplaces rocks with a flat-on-flat, not inclined, geometry (e.g., Schelling and Arita, 1991; Srivastava and Mitra, 1994; Robinson et al., 2006; McQuarrie et al., 2008; Long et al., 2011c). Second, an inclined slab predicts higher pressures in the north compared to the south, whereas for our data the distribution of P–T conditions is symmetric to the north and south of the Tethyan rocks (Fig. 4), which covers an across-strike distance of $\sim$60 km. Post-peak-metamorphic flattening (Fig. 5D), however, predicts exactly our observations: pressures are symmetric about the Tethyan rocks, and the pressure distribution is super-lithostatic. Chambers et al. (2009) and Lee et al. (2000) reached similar conclusions in NW India and southern Tibet, although with much sparser data.

In the context of THS–GHS exposures in eastern Bhutan, Chambers et al. (2011) argued that thinning might juxtapose hotter deeper GHS with cooler shallower THS, forcing prograde metamorphism of the THS as the section thins. This process is

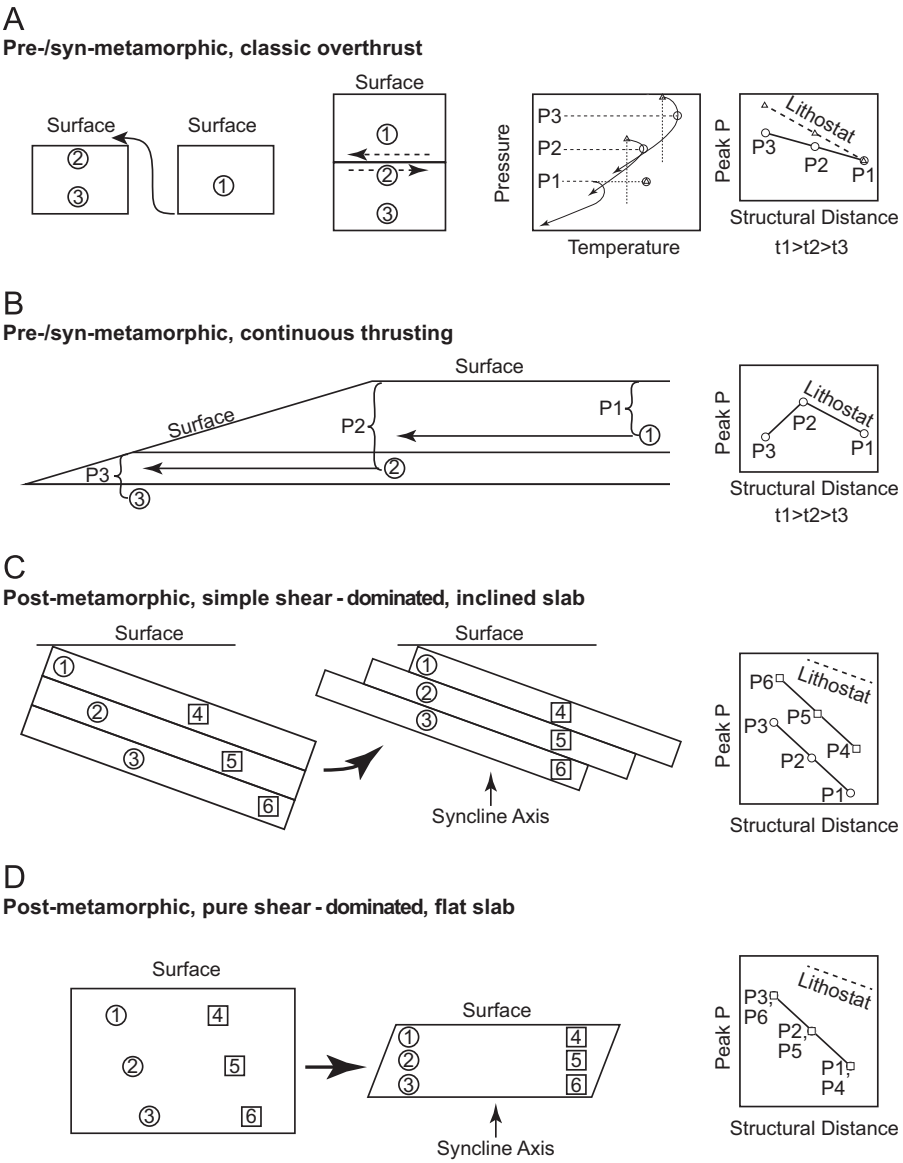

Fig. 5. Pressure–temperature consequences of different tectonic scenarios. (A) Classic instantaneous overthrust model predicts older ages for structurally higher (shallower) rocks, and a sublithostatic field gradient. Dotted lines show syn-thrusting *P–T* evolution. (B) Pre- to syn-metamorphic thrusting, typical for the Himalaya, predicts older ages for structurally higher rocks, a lithostatic pressure gradient towards the hinterland, and a flat or inverted pressure gradient towards the foreland. (C) Post-peak-metamorphic simple shear of an inclined slab produces a super-lithostatic pressure gradient, but a major pressure offset for rocks separated by a significant across-strike distance on either side of a syncline axis. (D) Post-peak-metamorphic pure shear-dominated flattening of a flat slab produces a super-lithostatic pressure gradient, and comparable pressures on opposite sides of a syncline axis.

similar to our interpretations, except that shallower rocks experience *syn*-prograde-metamorphic flattening, rather than post-peak-metamorphic flattening. Such a model should produce heating in the THS either isobarically or with a pressure decrease, however, and contrasts with the majority of our *P–T* paths that generally show heating with loading and with textures documenting extension after metamorphism (Long and McQuarrie, 2010; this study). Consequently, syn-prograde-metamorphic thinning might have occurred in eastern Bhutan, but does not explain the majority of our data from central Bhutan.

4.3. Implications for orogenesis

Although flattening has been recognized in previous microstructural studies in the Himalaya (Grujic et al., 1996; Grasemann et al., 1999; Law et al., 2004; Long et al., 2011a), the importance of this flattening to orogenesis may be questioned because of large extrapolations beyond individual hand samples and because the timing of flattening can be difficult to constrain. Based on microstructural measurements alone, it may be impossible to determine whether a deformed grain experienced flattening prior to, during, or after metamorphism. In contrast, our data indicate post-peak-metamorphic thinning of the section by an amount commensurate with structural measurements: the *P–T* data corroborate the c. 50% layer-normal flattening estimated from thin-section scale strain analysis (Long et al., 2011a), and imply that flattening textures were formed after the peak of metamorphism. Most data from Bhutan indicate the peak of prograde metamorphism at c. 20 Ma (e.g., Chambers et al., 2011; Kellett et al., 2010; Tobgay et al., 2012) and cooling through muscovite closure to Ar loss c. 10 Ma (Long et al., in review), implying that flattening occurred between 20 and 10 Ma. Taken together, these data suggest that flattening occurred during or immediately following displacement on the MCT and that the associated shear

contributes a few tens of km additional forward propagation of the base of the GHS relative to Tethyan rocks, similar to estimates of displacement on the STDS in the region (Long and McQuarrie, 2010).

In the context of structural semantics, some might argue that distributed top-to-the-north shear through most of the section indicates that the STDS occurs as a broad, ductile shear zone, originally nearly 20 km thick and now nearly 10 km thick. In general, we prefer to label structures based on zones of high shear strain, determined either directly through textures or from regional geological constraints such as stratigraphic repetitions or juxtapositions, pronounced metamorphic and chronologic gradients, etc. (see Kohn, 2008; Martin et al., 2005; Searle et al., 2008). Virtually all metamorphic rocks in the Himalaya are penetratively deformed to some degree. Identifying every such rock as a shear zone overlooks the fact that high-strain boundaries separate rock domains that have experienced low shear. In our view, the Shemgang section does not qualify for shear zone status. Regardless, our data indicate that the STDS does not propagate as a discrete shear horizon towards the foreland, in contrast to the channel flow and wedge insertion orogenic models.

Flattening and north-directed shear of Himalayan metamorphic rocks are generally interpreted as characteristic of ductile extrusion and channel flow (e.g., Vannay and Grasemann, 2001; Grujic et al., 2002; Law et al., 2004; Fig. 4A). However, published channel flow models show much more symmetric regions of north-directed and south-directed shear above and below the channel core, respectively (Grujic et al., 1996; Beaumont et al., 2001, 2004; Jamieson et al., 2004) than indicated in our study area (Long and McQuarrie, 2010; Long et al., 2011a). Changes to model parameters such as rock rheology or distribution of erosion might reconcile these differences. Whereas the lack of a major extensional shear zone or STDS between the GHS and Tethyan rocks is still compatible with numerical models that allow for limited (10's of kms) of STDS displacement (Jamieson et al., 2004), it varies significantly from the community's perception of channel flow, which promotes equal displacement on the MCT and STD (e.g., Cottle et al., 2007). Our data support limited (a few tens of km) channel flow (Long and McQuarrie, 2010)—only a few percent of total displacement on the basal Main Himalayan thrust (MHT). Flattening and north-directed flow of Tethyan rocks are at least equally consistent with critical taper, as a wedge-weakening event would cause flattening and extensional thinning (Fig. 4B; Northrup, 1996). Possible triggers include a reduction in basal friction, accumulation of partial melts beyond a critical threshold (e.g., Rosenberg and Handy, 2005), or underplating of thermally-weakened rocks (Northrup, 1996; Kohn and Corrie, 2011). Thinning could have been accommodated homogeneously, as observed in our study area, or heterogeneously, as observed farther north where a discrete STDS is evident. In the latter case, homogeneous thinning of the GHS would be balanced by extensional structures in Tethyan rocks, rooting into a master decollement—the STDS. The tectonic wedging model does not predict flattening, so is the least consistent with our observations (Fig. 3C).

Ultimately, attempting to contrast channel flow and critical taper may be counterproductive: both models are reconcilable with north- vs. south-directed flow at higher vs. lower structural levels respectively within the context of orogenic flattening and thinning. Rather than labeling this process "channel flow" vs. "critical taper", we recommend the less polarizing and more accurate term "orogenic flattening". This process readily explains the occurrence of thrust-sense and normal-sense shears (Burchfiel and Royden, 1985), metamorphic characteristics (Kohn, 2008; this study), and the parallelism of fabrics and bounding structures (Northrup, 1996). Orogenic flattening could range from pipe-flow exhibiting a neutral plane within the center of the flow field ("channel flow") to general shear involving additive simple and pure shear ("critical taper"). The asymmetry of flow and relatively small inferred displacement on the STDS in central Bhutan (Long and McQuarrie, 2010) fall much closer to the critical taper endmember of orogenic flattening than channel flow. A larger displacement on the STDS, e.g. $\geq$100 km, or documentation of sustained flow symmetry would more strongly support the channel flow endmember.

5. Conclusions

Our observations lead to 5 key conclusions:

1) Pressure, temperature, and *P*–*T* path continuity across lithologic contacts implies that the STDS is not present as a discrete structure in this area of the Himalaya (Long and McQuarrie, 2010).
2) A super-lithostatic pressure gradient is observed through the GHS and THS but cannot be explained by thrusting models.
3) The consistency of pressures for ~30 km on either side of a major upright syncline implies that rocks were metamorphosed essentially flat and later folded (cf. Gansser, 1983).
4) Post-peak-metamorphic flattening by c. 50% accompanied by distributed top-to-the-north shearing explains *P*–*T* distributions (this study) and microstructures (Long et al., 2011a).
5) Extrapolating to the north, the STDS can be understood as a strain incompatibility feature within the context of orogenic flattening (Burchfiel and Royden, 1985), with homogeneously vs. heterogeneously distributed strain towards the foreland vs. hinterland respectively.

Acknowledgments

We thank D. Ruscitto and F.J. Ryerson for their help with electron probe microanalysis, C.J. Northrup for tectonic discussions, and Dorji Wangda (the former Director General) of the Bhutan Department of Geology and Mines and Ugyen Wangda (Chief Geologist/Head) of the Geological Survey of Bhutan for permissions and support. Two anonymous reviews and comments from Alex Webb helped focus and clarify our thoughts and discussion. Funded by the NSF Grants EAR 1048124 to MJK and EAR 0738522 to NM.

Appendix A. Supporting information

Supplementary data associated with this article can be found in the online version at http://dx.doi.org/10.1016/j.epsl.2012.07.001.

References

Beaumont, C., Jamieson, R.A., Nguyen, M.H., Lee, B., 2001. Himalayan tectonics explained by extrusion of a low-viscosity crustal channel coupled to focused surface denudation. Nature 414, 738–742.

Beaumont, C., Jamieson, R.A., Nguyen, M.H., Medvedev, S., 2004. Crustal channel flows; 1, numerical models with applications to the tectonics of the Himalayan–Tibetan Orogen. J. Geophys. Res. 109, B06406, http://dx.doi.org/10.1029/2003JB002809.

Berman, R.G., 1990. Mixing properties of Ca–Mg–Fe–Mn garnets. Am. Mineral. 75 (328–244).

Bhargava, O.N., 1995. The Bhutan Himalaya: A Geological Account. Geological Survey of India Special Publication, vol. 39, pp. 1–245.

Burchfiel, B.C., Royden, L.H., 1985. North–south extension within the convergent Himalayan region. Geology 13, 679–682.

Chambers, J., Caddick, M., Argles, T., Horstwood, M., Sherlock, S., Harris, N., Parrish, R., Ahmad, T., 2009. Empirical constraints on extrusion mechanisms from the upper margin of an exhumed high-grade orogenic core, Sutlej valley, NW India. Tectonophysics 477, 77–92.

Chambers, J.A., Parrish, R., Argles, T., Harris, N., Horstwood, M., 2011. A short-duration pulse of ductile normal shear on the outer South Tibetan detachment in Bhutan: alternating channel flow and critical taper mechanics of the eastern Himalaya. Tectonics, 30, , http://dx.doi.org/10.1029/2010TC002784.

Corrie, S.L., Kohn, M.J., 2011. Metamorphic history of the central Himalaya, Annapurna region, Nepal, and implications for tectonic models. Geol. Soc. Am. Bull. 123, 1863–1879.

Cottle, J.M., Jessup, M.J., Newell, D.L., Searle, M.P., Law, R.D., Horstwood, M.S.A., 2007. Structural insights into the early stages of exhumation along an orogen-scale detachment: the South Tibetan Detachment System, Dzakaa Chu section, eastern Himalaya. J. Struct. Geol. 29, 1791–1797.

Cottle, J.M., Waters, D.J., Riley, D., Beyssac, O., Jessup, M.J., 2011. Metamorphic history of the South Tibetan Detachment System, Mt. Everest region, revealed by RSCM thermometry and phase equilibria modeling. J. Metamorph. Geol. 29, 561–582.

Dahlen, F.A., 1990. Critical taper model of fold-and-thrust belts and accretionary wedges. Ann. Rev. Earth Planet. Sci. 18, 55–99.

Daniel, C.G., Hollister, L.S., Parrish, R.R., Grujic, D., 2003. Exhumation of the Main Central Thrust from lower crustal depths, eastern Bhutan Himalaya. J. Metamorph. Geol. 21, 317–334.

Davidson, C., Grujic, D.E., Hollister, L.S., Schmid, S.M., 1997. Metamorphic reactions related to decompression and synkinematic intrusion of leucogranite, High Himalayan Crystallines, Bhutan. J. Metamorph. Geol. 15, 593–612.

Davis, D., Suppe, J., Dahlen, F.A., 1983. Mechanics of fold-thrust belts and accretionary wedges. J. Geophys. Res. 88, 1153–1172.

England, P.C., Thompson, A.B., 1984. Pressure–temperature–time paths of regional metamorphism, Part I: heat transfer during the evolution of regions of thickened continental crust. J. Petrol. 25, 894–928.

Ferry, J.M., Spear, F.S., 1978. Experimental calibration of partitioning of Fe and Mg between biotite and garnet. Contrib. Mineral. Petrol. 66, 113–117.

Florence, F.P., Spear, F.S., 1991. Effects of diffusional modification of garnet growth zoning on *P–T* path calculations. Contrib. Mineral. Petrol. 107, 487-500 .

Florence, F.P., Spear, F.S., Kohn, M.J., 1993. *P–T* paths from northwestern New Hampshire: metamorphic evidence for stacking in a thrust/nappe complex. Am. J. Sci. 293, 939–979.

Gansser, A., 1983. Geology of the Bhutan Himalaya. Burkhäuser Verlag, Zurich.

Godin, L., Grujic, D., Law, R.D., Searle, M.P., 2006. Channel flow, ductile extrusion and exhumation in continental collision zones; an introduction. In: Law, R.D., Searle, M.P., Godin, L. (Eds.), Channel Flow, Ductile Extrusion and Exhumation in Continental Collision Zones, pp. 1–23 (Geological Society Special Publication).

Graham, C.M., Powell, R., 1984. A garnet-hornblende geothermometer: calibration, testing, and application to the Pelona Schist, Southern California. J. Metamorph. Geol. 2, 13–31.

Grasemann, B., Fritz, H., Vannay, J.-C., 1999. Quantitative kinematic flow analysis from the Main Central Thrust Zone (NW-Himalaya, India); implications for a decelerating strain path and the extrusion of orogenic wedges. J. Struct. Geol. 21, 837–853.

Grujic, D., Casey, M., Davidson, C., Hollister, L.S., Kuendig, R., Pavlis, T.L., Schmid, S.M., 1996. Ductile extrusion of the Higher Himalayan Crystalline in Bhutan; evidence from quartz microfabrics. Tectonophysics 260, 21–43.

Grujic, D., Hollister, L.S., Parrish, R.R., 2002. Himalayan metamorphic sequence as an orogenic channel: insight from Bhutan. Earth Planet. Sci. Lett. 198, 177–191.

Henry, P., LePichon, X., Goffé, B., 1997. Kinematic, thermal and petrological model of the Himalayas: constraints related to metamorphism within the under-thrust Indian crust and topographic evolution. Tectonophysics 273, 31–56.

Herman, F., Copeland, P., Avouac, J.-P., Bollinger, L., Mahéo, G., Le Fort, P., Rai, S., Foster, D., Pecher, A., Stüwe, K., Henry, P., 2010. Exhumation, crustal deformation, and thermal structure of the Nepal Himalaya derived from inversion of thermochronological and thermobarometric data and modeling of the topography. J. Geophys. Res., 115, http://dx.doi.org/10.1029/2008/JB006126.

Hoisch, T.D., 1990. Empirical calibration of six geobarometers for the mineral assemblage quartz+muscovite+biotite+plagioclase+garnet. Contrib. Mineral. Petrol. 104, 225–234.

Jamieson, R.A., Beaumont, C., Medvedev, S., Nguyen, M.H., 2004. Crustal channel flows; 2, numerical models with implications for metamorphism in the Himalayan–Tibetan Orogen. J. Geophys. Res., 109, http://dx.doi.org/10.1029/2003JB002811.

Kellett, D.A., Grujic, D., Warren, C., Cottle, J., Jamieson, R., Tenzin, T., 2010. Metamorphic history of a syn-convergent orogen-parallel detachment: the South Tibetan detachment system, Bhutan Himalaya. J. Metamorph. Geol. 28, 785–808.

Kellett, D.A., Grujic, D., 2012. New insight into the South Tibetan detachment system: not a single progressive deformation. Tectonics, 31, http://dx.doi.org/10.1029/2011TC002957.

Kohn, M.J., 2008. *P–T–t* data from central Nepal support critical taper and repudiate large-scale channel flow of the Greater Himalayan Sequence. Geol. Soc. Am. Bull. 120, 259–273, http://dx.doi.org/10.1130/b26252.1.

Kohn, M.J., Corrie, S.L., 2011. Preserved Zr-temperatures and U–Pb ages in high-grade metamorphic titanite: evidence for a static hot channel in the Himalayan orogen. Earth Planet. Sci. Lett. 311, 136–143.

Kohn, M.J., Spear, F.S., 1990. Two new geobarometers for garnet amphibolites, with applications to southeastern Vermont. Am. Mineral. 75, 89–96.

Kohn, M.J., Spear, F.S., 2000. Retrograde net transfer reaction insurance for *P–T* estimates. Geology 281, 127–1130.

Kohn, M.J., Orange, D.L., Spear, F.S., Rumble, D., Harrison, T.M., 1992. Pressure, temperature, and structural evolution of west-central New Hampshire: hot thrusts over cold basement. J. Petrol. 33, 521–556.

Kohn, M.J., Spear, F.S., Dalziel, I.W.D., 1993. Metamorphic *P–T* paths from Cordillera Darwin, a core complex in Tierra del Fuego, Chile. J. Petrol. 34, 519–542.

Kohn, M.J., Wieland, M.S., Parkinson, C.D., Upreti, B.N., 2004. Miocene faulting at plate tectonic velocity in the Himalaya of central Nepal. Earth Planet. Sci. Lett. 228, 299–310.

Koziol, A.M., Newton, R.C., 1988. Redetermination of the anorthite breakdown reaction and improvement of the plagioclase–garnet–Al_2SiO_5–quartz geobarometer. Am. Mineral. 73, 216–223.

Law, R.D., Searle, M.P., Simpson, R.L., 2004. Strain, deformation temperatures and vorticity of flow at the top of the Greater Himalayan Slab, Everest Massif, Tibet. J. Geol. Soc. London 161, 305–320.

Lee, J., Hacker, B.R., Dinklage, W.S., Wang, Y., Gans, P., Calvert, A., Wan, J., Chen, W., Blythe, A.E., McClelland, W.C., 2000. Evolution of the Kangmar Dome, southern Tibet; structural, petrologic, and thermochronologic constraints. Tectonics 19, 872–895.

Long, S., McQuarrie, N., 2010. Placing limits on channel flow: insights from the Bhutan Himalaya. Earth Planet. Sci. Lett. 290, 375–390.

Long, S., McQuarrie, N., Tobgay, T., Hawthorne, J., 2011a. Quantifying internal strain and deformation temperature in the eastern Himalaya, Bhutan: implications for the evolution of strain in thrust sheets. J. Struct. Geol. 33, 579–608.

Long, S., McQuarrie, N., Tobgay, T., Grujic, D., Hollister, L., 2011b. Geologic map of Bhutan. J. Maps 2011, 184–192.

Long, S., McQuarrie, N., Tobgay, T., Grujic, D., 2011c. Geometry and crustal shortening of the Himalayan fold-thrust belt, eastern and central Bhutan. Geol. Soc. Am. Bull. 123, 1427–1447, http://dx.doi.org/10.1130/B30203.1.

Long, S.P., McQuarrie, N., Tobgay, T., Coutand, I., Cooper, F.J., Reiners, P.W., Wartho, J.-A., Hodges, K.V. Variable shortening rates in the eastern Himalayan thrust belt, Bhutan: insights from multiple thermochronologic and geochronologic datasets tied to kinematic reconstructions. Tectonics, in review.

Martin, A.J., DeCelles, P.G., Gehrels, G.E., Patchett, P.J., Isachsen, C., 2005. Isotopic and structural constraints on the location of the Main Central thrust in the Annapurna Range, central Nepal Himalaya. Geol. Soc. Am. Bull. 117, 926–944.

McQuarrie, N., Robinson, D., Long, S., Tobgay, T., Grujic, D., Gehrels, G., Ducea, M., 2008. Preliminary stratigraphic and structural architecture of Bhutan: implications for the along strike architecture of the Himalayan system. Earth Planet. Sci. Lett. 272, 105–117.

Northrup, C.J., 1996. Structural expressions and tectonic implications of general noncoaxial flow in the midcrust of a collisional orogen: the northern Scandinavian Caledonides. Tectonics 15, 490–505.

Robinson, D.M., DeCelles, P.G., Copeland, P., 2006. Tectonic evolution of the Himalayan thrust belt in western Nepal: implications for channel flow models. Geol. Soc. Am. Bull. 118, 865–885.

Rosenberg, C.L., Handy, M.R., 2005. Experimental deformation of partially melted granite revisited; implications for the continental crust. J. Metamorph. Geol. 23, 19–28.

Rowley, D.B., 1996. Age of initiation of collision between India and Asia; a review of stratigraphic data. Earth Planet. Sci. Lett. 145, 1–13.

Royden, L.H., 1993. The steady state thermal structure of eroding orogenic belts and accretionary prisms. J. Geophys. Res. B Solid Earth Planets 98, 4487–4507.

Schelling, D., Arita, K., 1991. Thrust tectonics, crustal shortening, and the structure of the far-eastern Nepal Himalaya. Tectonics 10, 851–862.

Searle, M.P., Law, R.D., Godin, L., Larson, K.P., Streule, M.J., Cottle, J.M., Jessup, M.J., 2008. Defining the Himalayan Main Central thrust in Nepal. J. Geol. Soc. London 165, 523–534.

Spear, F.S., 1991. On the interpretation of peak metamorphic temperatures in the of garnet diffusion during cooling. J. Metamorph. Geol. 9, 379–388.

Spear, F.S., 1995. Metamorphic Phase Equilibria and Pressure–Temperature–Time Paths, 2nd ed. Mineralogical Society of America, Washington, D.C.

Spear, F.S., Kohn, M.J., Florence, F.P., Menard, T., 1990a. A model for garnet and plagioclase growth in pelitic schists: implications for thermobarometry and *P–T* path determinations. J. Metamorph. Geol. 8, 683–696.

Spear, F.S., Hickmott, D.D., Selverstone, J., 1990b. Metamorphic consequences of thrust emplacement, Fall Mountain, New Hampshire. Geol. Soc. Am. Bull. 102, 1344–1360.

Spear, F.S., Kohn, M.J., Cheney, J.T., 1999. *P–T* paths from anatectic pelites. Contrib. Mineral. Petrol. 134, 17–32.

Srivastava, P., Mitra, G., 1994. Thrust geometries and deep structure of the outer and lesser Himalaya, Kumaon and Garwal (India): implications for evolution of the Himalayan fold-and-thrust belt. Tectonics 13, 89–109.

Tobgay, T., McQuarrie, N., Long, S., Kohn, M.J., Corrie, S.L., 2012. The age and rate of displacement along the Main Central Thrust in the western Bhutan Himalaya. Earth Planet. Sci. Lett. 319–320, 146–158.

Tomkins, H.S., Powell, R., Ellis, D.J., 2007. The pressure dependence of the zirconium-in-rutile thermometer. J. Metamorph. Geol. 25, 703–713.

Vannay, J.-C., Grasemann, B., 2001. Himalayan inverted metamorphism and syn-convergence extension as a consequence of a general shear extrusion. Geol. Mag. 138, 253–276.

Watson, E.B., Wark, D.A., Thomas, J.B., 2006. Crystallization thermometers for zircon and rutile. Contrib. Mineral. Petrol. 151, 413–433.

Webb, A.A.G., Yin, A., Harrison, T.M., Celerier, J., Burgess, W.P., 2007. The leading edge of the Greater Himalayan Crystalline complex revealed in the NW Indian Himalaya: implications for the evolution of the Himalayan orogen. Geology 35, 955–958.